

Supplementary Materials for **Susceptible supply limits the role of climate in the early SARS-CoV-2 pandemic**

Rachel E. Baker*, Wenchang Yang, Gabriel A. Vecchi, C. Jessica E. Metcalf, Bryan T. Grenfell

*Corresponding author. Email: racheleb@princeton.edu

Published 18 May 2020 on *Science* First Release
DOI: 10.1126/science.abc2535

This PDF file includes:

Materials and Methods
Figs. S1 to S11
References

Other Supporting Online Material for this manuscript includes the following:
(available at science.sciencemag.org/cgi/content/full/science.abc2535/DC1)

MDAR Reproducibility Checklist (.pdf)

Materials and Methods

Data

Data on endemic coronaviruses come from The National Respiratory and Enteric Virus Surveillance System (NREVSS) (19) and are available on application after signing a data-use agreement with the Center for Disease Control. NREVSS is a passive surveillance network, established by the CDC that collects data from multiple laboratories across the US (25). The dataset contains the number of total weekly tests and the number of positive tests for each of the four coronavirus strains: HKU1, OC43, NL63, 229E. However, no details are provided on the number or location of reporting laboratories each week and year-to-year changes in reporting are possible. To partially correct for this, we calculate percentage positive cases for HKU1 and OC43 and following (18), we multiply this number by the proportion of weekly ILI visits obtained from the US Outpatient Influenza-like Illness Surveillance Network (ILINet). Given year-to-year variability may still not be reflective of true variability in coronavirus cases, we fit our model using only mean climatology to capture broad patterns of seasonal dynamics and timing.

Climate data for the US regions come from ERA5 (20) and population-weighted averages of specific humidity over the census region area are constructed using 2015 population data from CIESIN (21). We calculate the average climatology for 2014-2020 to run the model and do not consider year-to-year climate variations. For simulating global pandemics, we calculate a 30 year climatology using specific humidity from NASA's Modern-Era Retrospective analysis for Research and Applications (MERRA) dataset (27).

Model

The climate-driven SIRS model is based on (12):

$$\frac{dS}{dT} = \frac{N - S - I}{L} - \frac{\beta(t)IS}{N} \quad (1)$$

$$\frac{dI}{dT} = \frac{\beta(t)IS}{N} - \frac{I}{D} \quad (2)$$

where S is the susceptible population, I is the number of infectious individuals and N is the population. L represents the duration of immunity and D is the mean infectious period (fixed at 5 days). $\beta(t)$ is the contact rate at time t and is related to the basic reproductive number by $R_0(t) = \beta(t)D$. R_0 is related to specific humidity $q(t)$ using the equation:

$$R_0(t) = \exp(a * q(t) + \log(R_{0max} - R_{0min})) + R_{0min} \quad (3)$$

where a is the climate dependence parameter and R_{0max} , R_{0min} are the maximum and minimum reproductive numbers respectively.

Fitting the model

For OC43 and HKU1 we find a and L by fitting the model to data from census regions in the US. We take the average fit across census regions to represent the OC43 and HKU1 values of a and L . In general, parameter values for each disease show agreement across census regions. The western region is a slight outlier for both diseases. As this region pools data from both Alaska and Hawaii (as well as western US states) it represents a large range of climatologies and this likely makes the true climate effect harder to disentangle.

We fit over a range of climate dependencies reflecting no climate dependence to approximately double the known climate dependence on influenza [0,300]. The immunity length of SARS-CoV-2 is yet to be determined, however, some early stage research found that rhesus macaques could not be reinfected 30 days post-infection (28). Studies using another endemic

coronavirus, NL63, found that neutralizing antibody titers declined to zero 52 weeks after first infection (29). Using the US betacoronavirus data, another modelling effort found an immunity length of 40 weeks (18). Here, we assume 20 weeks in the lower bound on immunity length, and allow the model to fit a maximum immunity length of two years. Our fitted immunity lengths, L , are 62.5 and 66.25 weeks for OC43 and HKU1 respectively. Our fitted values for a are -32.5 and -227.5 for OC43 and HKU1 respectively. Visualization of the fitting process is shown in Fig. S2 and S3. For influenza, we use climate dependencies from earlier work (12), where a is -180 and L we fix at 40 weeks. Immunity for influenza is complicated by the evolution of the virus, however, 40 weeks leads to annual outbreaks without biennial dynamics and therefore provides a representation of influenza type-dynamics.

When fitting the model we use $R_{0min} = 1.2$, $R_{0max} = 2$, where R_{0min} represents a 40% reduction for R_{0max} , which is consistent with a potential maximum climate effect in other studies (18,20). We find these values of R_{0min} and R_{0max} are able to capture both the annual and biennial dynamics of OC43 and HKU1 respectively. When simulating a SARS-CoV-2 outbreak, we assume a slightly larger R_0 , corresponding to preliminary studies of the outbreak.

We run the model for fifty years to remove initial transient dynamics before fitting to case data. For the endemic model, to more accurately capture longer term susceptible dynamics, we assume a birth rate equal to the average weekly birth rate in the US between 2013 and 2020 taken from World Bank data. We set the birth rate equal to the mortality rate. We scale the model output to the census region data by first dividing both time series by the range of weekly cases and then set the model mean cases equal to the region data. This assumes a constant reporting rate for each region. Scaled data is shown in Figure S2 and Figure S3. Our fit statistic is the sum of the absolute errors. To avoid overfitting to zero cases and low level stochastic observations, for instance at the start of the time series, we only measure errors when scaled cases exceed 5%. This ensures our models captures broadly peak timing and dynamics.

Model simulations

For simulations of SARS-CoV-2, we assume the climate modulates R_0 between a maximum of 2.5 and a minimum of 1.5, representing a 40% reduction in transmission at maximum (18,20). Prior work for the endemic coronaviruses suggests a lower R_{0max} of 2.2 (18), however, early reports for SARS-CoV-2 suggest higher values, closer to 2.9 (22). Here we choose a $R_{0max} = 2.5$ as a conservative upper bound. Only locations with very dry conditions (low specific humidity) will experience R_{0max} close to this limit. Model results using other R_0 values are shown in the sensitivity analysis. We do not consider birth rates when simulating the pandemic outbreak. Birth rates do not likely contribute to susceptible dynamics over the short-run and may complicate the interpretation of regional climate differences. In all simulations unless otherwise stated the model simulation starts on day 1 of the year, assuming 1/8e06 infected, no recovered and N-I susceptible.

In some analyses, we simulate the model in the general case using a sinusoidal function to capture seasonality in specific humidity. The sine function has the mean and temporal pattern of New York specific humidity, but the range of humidity values is allowed to vary.

Sensitivity analysis

The dependence of SARS-CoV-2 transmission on the climate is fundamentally unknown. Our three scenarios (influenza, OC43 and HKU1) represent a wide range of potential climate dependencies, with HKU1 showing more substantial variations in peak incidence across regions, and OC43 showing very little. Using these parameters, our simulations predict significant outbreaks across all locations. We further test the sensitivity of our results to potential changes in climate dependence, immunity length, R_0 and weather variability.

In Fig. S7, we run simulations varying the strength of climate dependence (from double our maximum estimated value to 0) and the humidity range (assuming mean humidity and seasonal

timing of New York). Across columns we vary the starting fraction of susceptibles from 1 to 0.7. Across rows we consider different values for minimum and maximum R_0 with scenarios representing our current values for SARS-CoV-2, values from (18), our endemic coronavirus values, and a more extreme scenario where $R_{0min} = 1$. The time series show a five year simulation for New York and Jakarta with the HKU1 (strong) climate dependence and starting susceptibility at 0.7 or 1.

In all cases, comparing across columns, reducing susceptibility to 0.7 substantially reduced pandemic peak size in the first year. Scenario b), where $R_{0max} = 2, R_{0min} = 1.2$ results in smaller outbreaks in both New York and Jakarta, though the size of the outbreaks relative to each other are similar to our baseline scenario, suggesting that even with these lower R_0 values, if a large outbreak occurs in New York, a similar sized outbreak may occur in this more tropical city. The only case where outbreaks do not occur in tropical regions is scenario d), when high specific humidity lowers R_0 to 1. In Fig. S8, we further test these implications of R_{0min} . In this analysis we fix $R_{0max} = 2.5$ and vary R_{0min} as a percentage reduction in R_{0max} . For the weak climate dependence scenario, OC43, changes to R_{0min} have minimal affect on peak size. For HKU1, when $R_{0min} \leq 1$, outbreaks do not occur in tropical locations.

We also consider the effect of different weather variability on pandemic peak size. Our main model uses mean specific humidity over a 30 year period, however this long-run mean smooths over the potential impact of year-to-year weather variability. We run our model using each individual year from the MERRA dataset, repeating the weather from that year for a 10 year period. Fig S9 and S10 show the results for HKU1 and OC43 parameters respectively. We find that across a range of locations, changes to weather variability do not alter the timing or intensity of the pandemic peak. However, endemic cycles exhibit much higher sensitivity to weather variation.

Finally, we also consider the potential effect of immunity length on pandemic peak size (Fig

S11). Immunity length does not influence the size of the pandemic peak, though will impact the timing of latter stage outbreaks.

Supplemental Figures

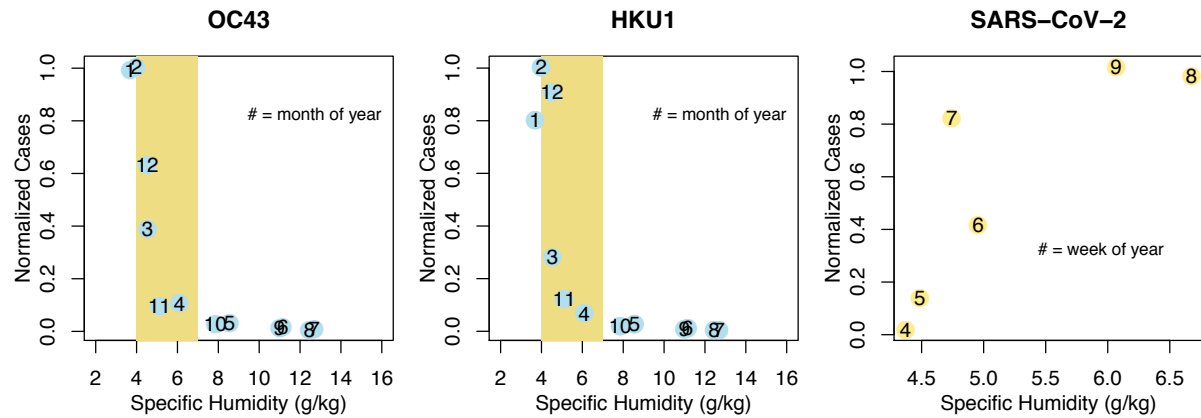


Figure S1: Seasonality of coronaviruses. Average monthly specific humidity plotted against normalized (between 0 and 1) cases of OC43 and HKU1 averaged across the US from 2014-2020, as well as normalized cases of SARS-CoV-2 in Wuhan from weeks 4-9 of 2020 (based on the time series available from the John Hopkins Coronavirus resource center at the time of access). The yellow shaded area in the first two plots corresponds to the width of the x-axis in the final plot, for comparison.

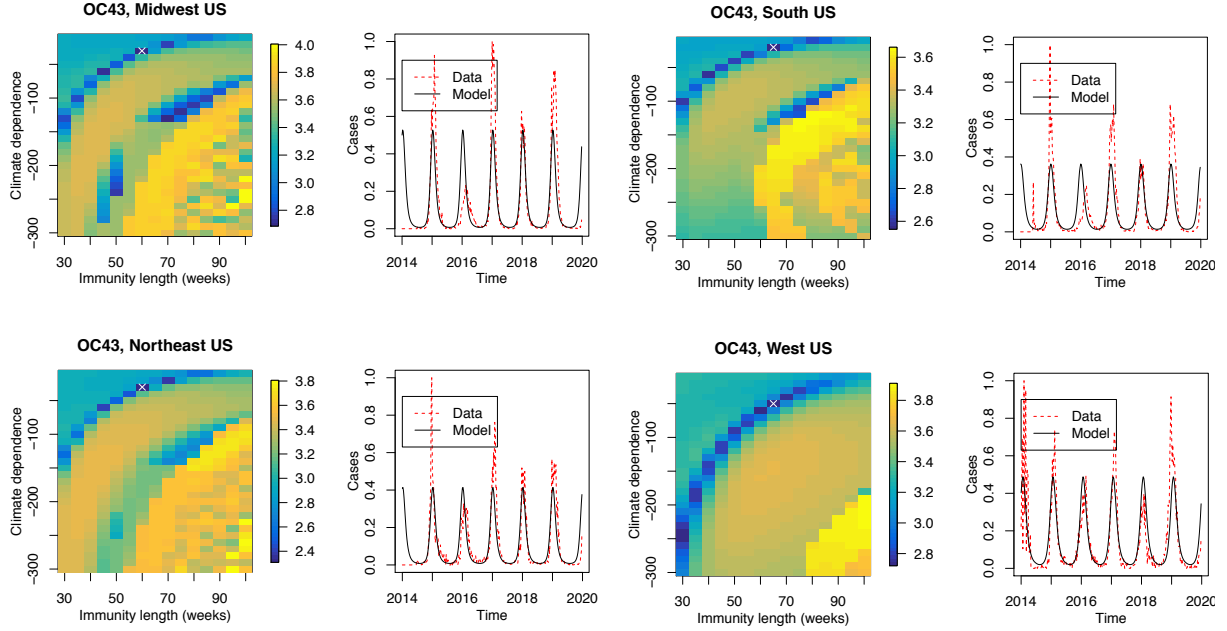


Figure S2: Model fit for OC43. Two parameters are fitted (climate dependence and immunity length) using case data for OC43 in four US census regions. Our model fits only the average seasonality of OC43 cases and does not take into account year-to-year variation. The surface plot shows the (logged) sum of absolute error. Darker regions represent a better fit of our model and the best fit parameters are shown with a white cross.

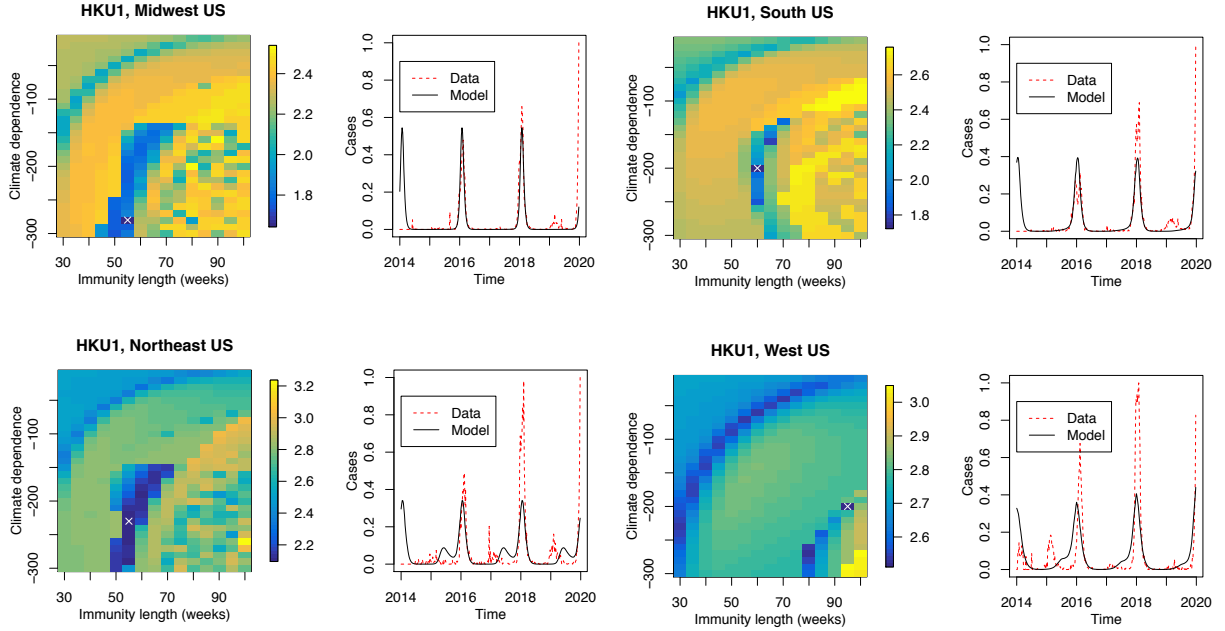


Figure S3: Model fit for HKU1. Two parameters are fitted (climate dependence and immunity length) using case data for HKU1 in four US census regions. Our model fits only the average seasonality of HKU1 cases and does not take into account year-to-year variation. The surface plot shows the (logged) sum of absolute error. Darker regions represent a better fit of our model and the best fit parameters are shown with a white cross.

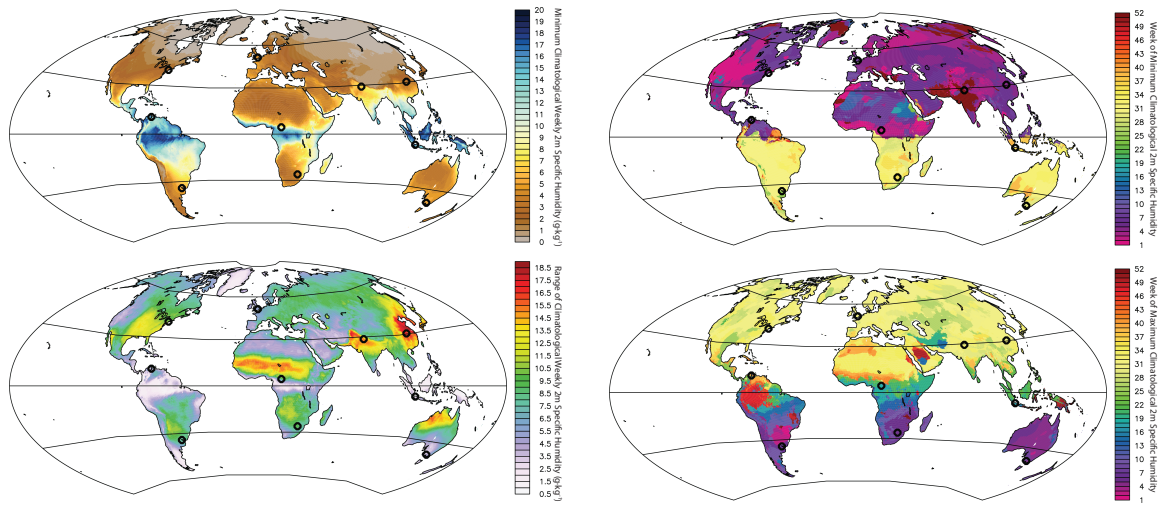


Figure S4: Specific humidity climatology. Minimum specific humidity and range of specific humidity as well as timing of minimum and maximum specific humidity is shown for the globe.

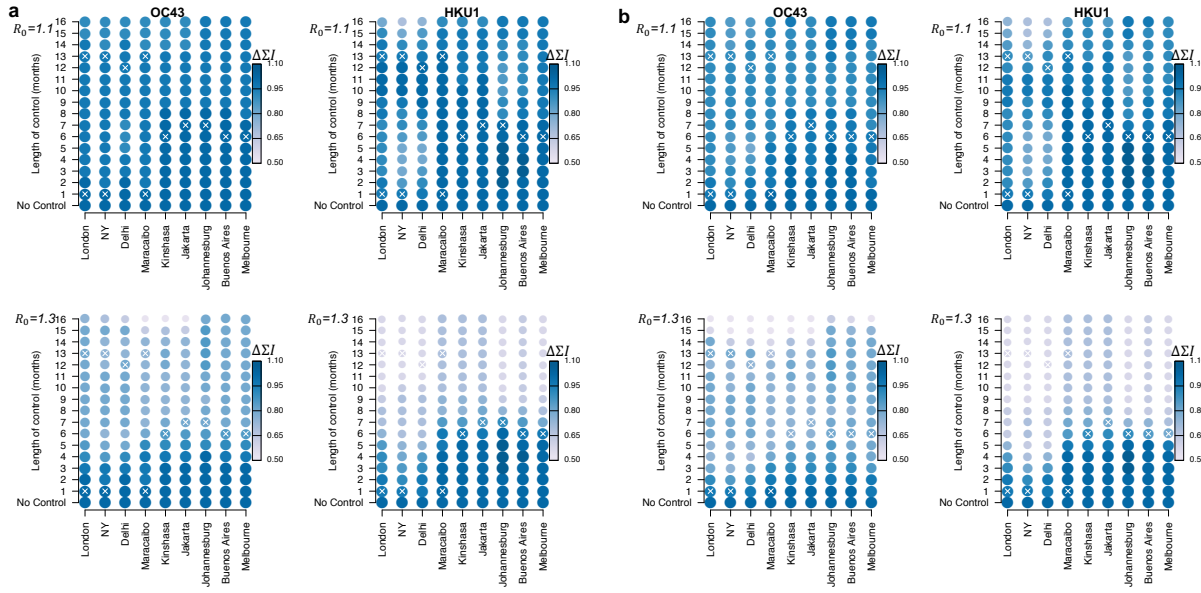


Figure S5: Impact of control on total infected. The relative (to the no-control scenario) effect of control measures on cumulative total infections by location where control measures begin at a) one month after the first infection or b) six weeks after the first infection.

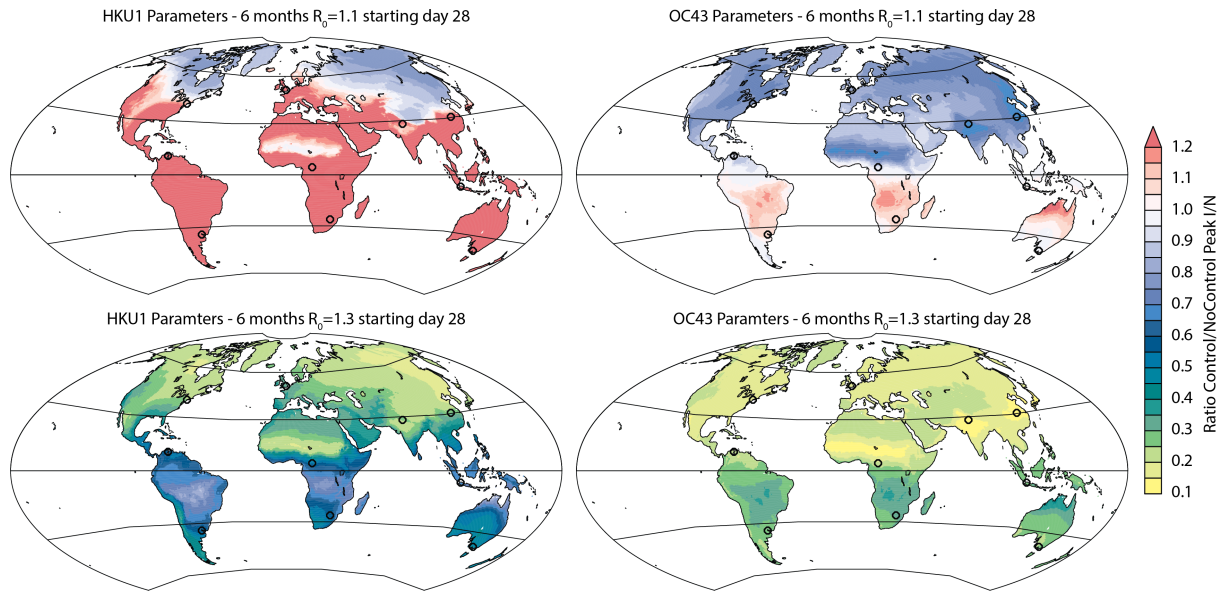


Figure S6: Map of relative I/N with control efforts at six months.) Map of relative change in peak incidence after six-months of controls using both the HKU1 and OC43 scenarios when $R_0 = 1.1$ and $R_0 = 1.3$.

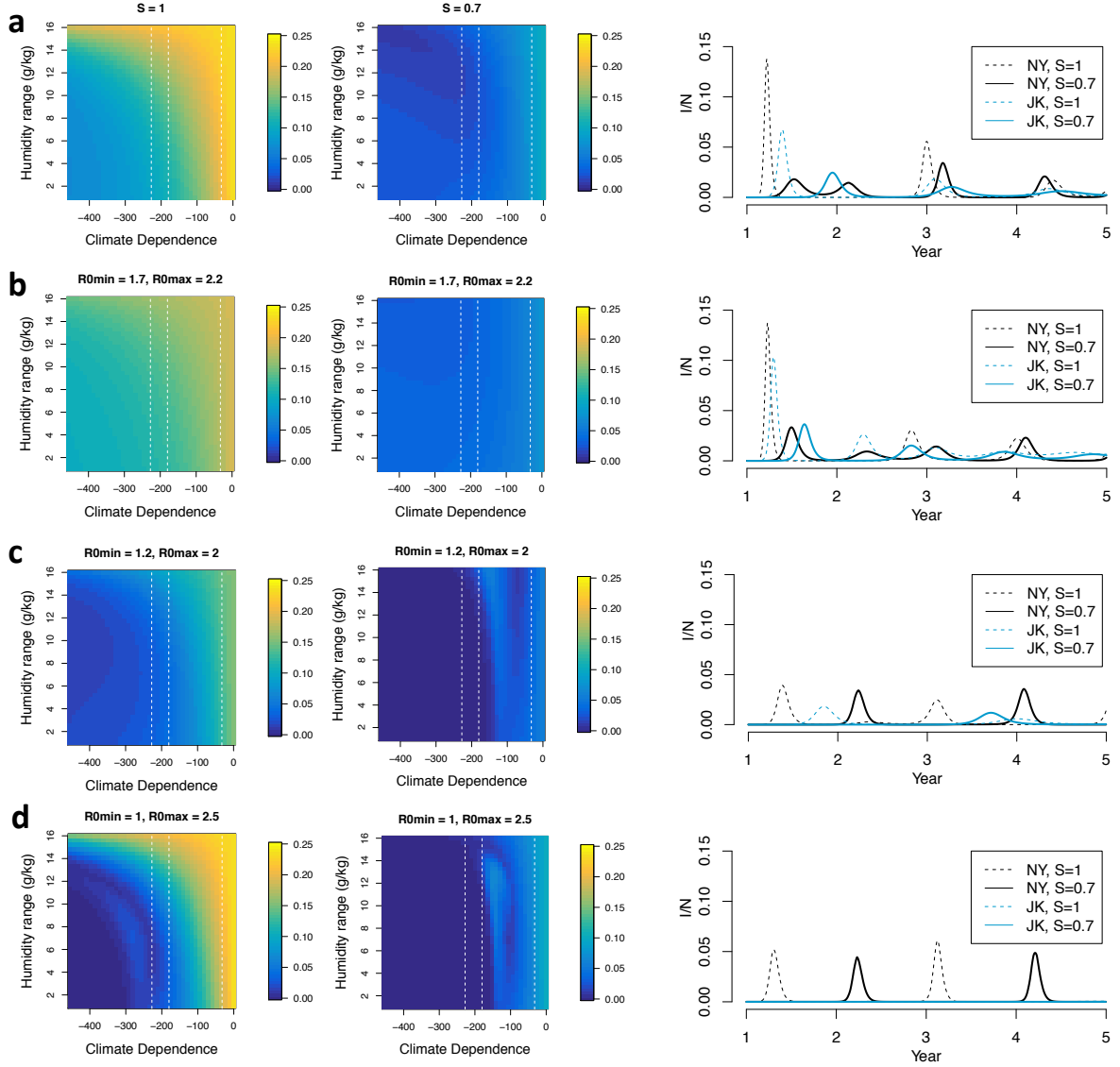


Figure S7: Sensitivity analysis. Image plots show peak I/N (within the six months) for different levels of climate dependence and humidity range with the proportion susceptible at the start of the simulation set to 1 (first column) or 0.7 (second column). The climate dependencies used in the scenarios in the main paper are shown with dashed lines. Values of R_{0min} and R_{0max} are allowed to vary across rows using a) $R_{0min} = 1.5, R_{0max} = 2.5$ i.e. our main model b) $R_{0min} = 1.7, R_{0max} = 2.2$ c) $R_{0min} = 1.2, R_{0max} = 2$ d) $R_{0min} = 1, R_{0max} = 2.5$. Simulated time series for New York (black) and Jakarta (blue) when $S = 1$ (dashed) and $S = 0.7$ (solid) and climate dependence/immunity is the same as HKU1 are shown in the right column.

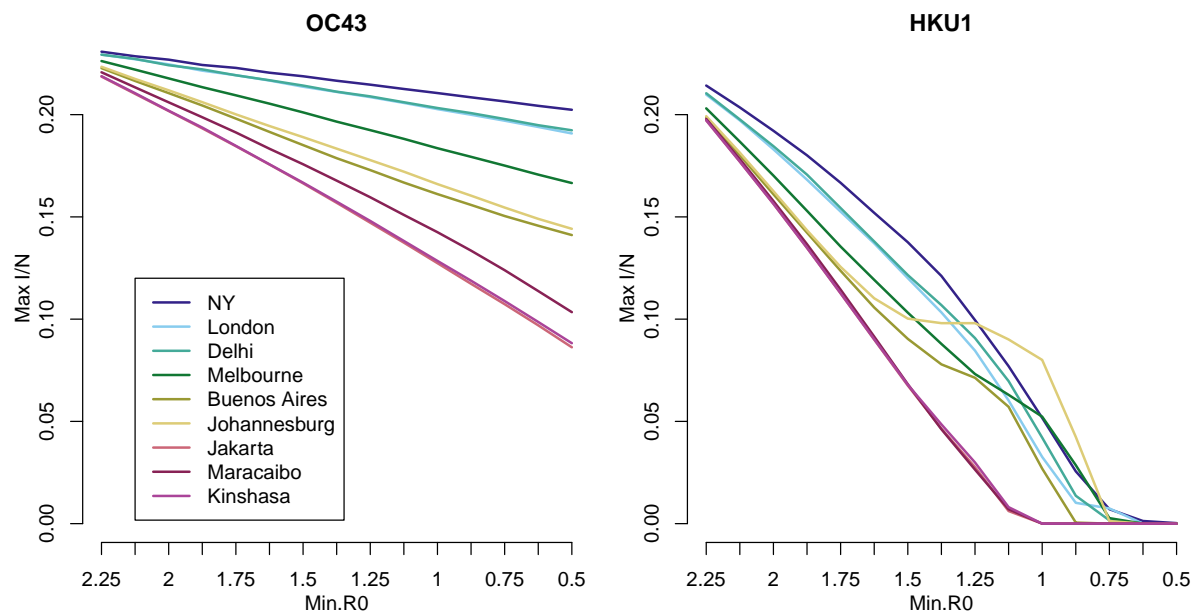


Figure S8: Sensitivity analysis. The effect of varying $R_{0\min}$ on peak I/N in the first year for different locations using OC43 and HKU1 climate dependence. $R_{0\max}$ is fixed at 2.5 and $R_{0\min}$ is varied.

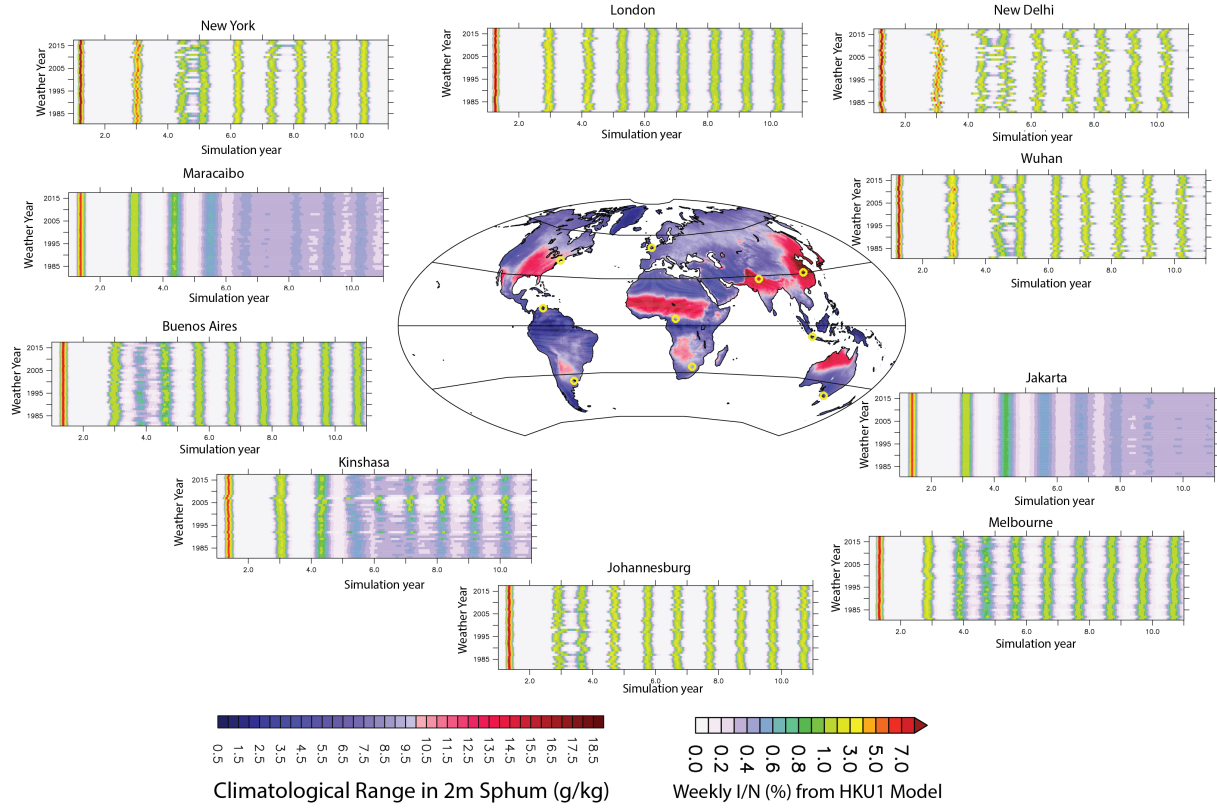


Figure S9: Sensitivity analysis. The effect of weather variability on pandemic peak size and endemic cycles, using HKU1 climate dependence.

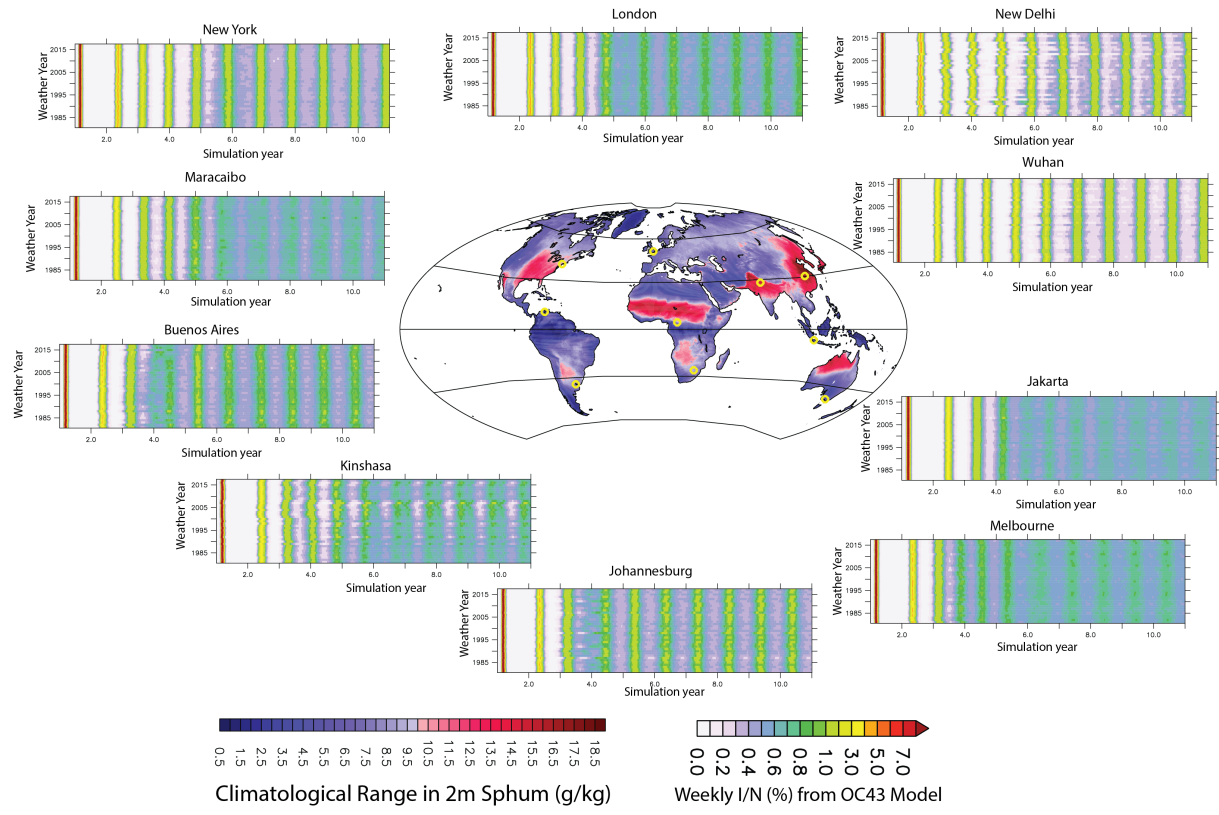


Figure S10: Sensitivity analysis. The effect of weather variability on pandemic peak size and endemic cycles, using OC43 climate dependence.

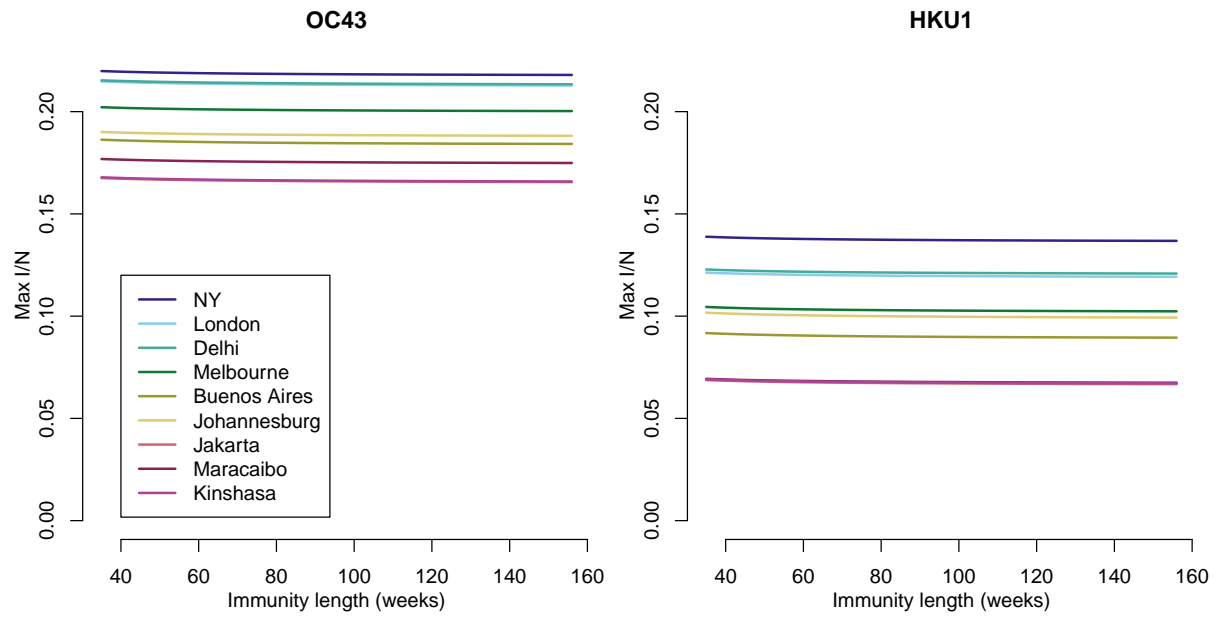


Figure S11: Sensitivity analysis. The effect of varying immunity length on peak I/N in the first year for different locations using OC43 and HKU1 climate dependence.

References and Notes

1. R. Verity, L. C. Okell, I. Dorigatti, P. Winskill, C. Whittaker, N. Imai, G. Cuomo-Dannenburg, H. Thompson, P. Walker, H. Fu, A. Dighe, J. Griffin, A. Cori, M. Baguelin, S. Bhatia, A. Boonyasiri, Z. M. Cucunuba, R. Fitzjohn, K. A. M. Gaythorpe, W. Green, A. Hamlet, W. Hinsley, D. Laydon, G. Nedjati-Gilani, S. Riley, S. van-Elsland, E. Volz, H. Wang, Y. Wang, X. Xi, C. Donnelly, A. Ghani, N. Ferguson, Estimates of the severity of COVID-19 disease. medRxiv 2020.03.09.20033357 [Preprint]. 13 March 2020; <https://doi.org/10.1101/2020.03.09.20033357>.
2. R. Li, C. Rivers, Q. Tan, M. B. Murray, E. Toner, M. Lipsitch, The demand for inpatient and ICU beds for COVID-19 in the US: lessons from Chinese cities. medRxiv 2020.03.09.20033241 [Preprint]. 16 March 2020; <https://doi.org/10.1101/2020.03.09.20033241>.
3. Q. Bukhari, Y. Jameel, Will coronavirus pandemic diminish by summer? SSRN 3556998 [Preprint]. 17 March 2020; <https://dx.doi.org/10.2139/ssrn.3556998>.
4. J. Wang, K. Tang, K. Feng, W. Lv, High temperature and high humidity reduce the transmission of COVID-19. SSRN 3551767 [Preprint]. 9 March 2020; <https://dx.doi.org/10.2139/ssrn.3551767>.
5. M. M. Sajadi, P. Habibzadeh, A. Vintzileos, S. Shokouhi, F. Miralles-Wilhelm, A. Amoroso, Temperature, humidity and latitude analysis to predict potential spread and seasonality for COVID-19. SSRN 3550308 [Preprint]. 5 March 2020; <https://dx.doi.org/10.2139/ssrn.3550308>.
6. W. Luo, M. S. Majumder, D. Liu, C. Poirier, K. D. Mandl, M. Lipsitch, M. Santillana, The role of absolute humidity on transmission rates of the COVID-19 outbreak. medRxiv 2020.02.12.20022467 [Preprint]. 17 February 2020; <https://doi.org/10.1101/2020.02.12.20022467>.
7. Y. Ma, Y. Zhao, J. Liu, X. He, B. Wang, S. Fu, J. Yan, J. Niu, B. Luo, Effects of temperature variation and humidity on the mortality of COVID-19 in Wuhan. medRxiv 2020.03.15.20036426 [Preprint]. 18 March 2020; <https://doi.org/10.1101/2020.03.15.20036426>.
8. R. E. Baker, A. S. Mahmud, C. J. E. Metcalf, Dynamic response of airborne infections to climate change: Predictions for varicella. *Clim. Change* **148**, 547–560 (2018). [doi:10.1007/s10584-018-2204-4](https://doi.org/10.1007/s10584-018-2204-4)
9. J. Shaman, M. Kohn, Absolute humidity modulates influenza survival, transmission, and seasonality. *Proc. Natl. Acad. Sci. U.S.A.* **106**, 3243–3248 (2009). [doi:10.1073/pnas.0806852106](https://doi.org/10.1073/pnas.0806852106) [Medline](#)
10. A. C. Lowen, J. Steel, Roles of humidity and temperature in shaping influenza seasonality. *J. Virol.* **88**, 7692–7695 (2014). [doi:10.1128/JVI.03544-13](https://doi.org/10.1128/JVI.03544-13) [Medline](#)
11. A. C. Lowen, S. Mubareka, J. Steel, P. Palese, Influenza virus transmission is dependent on relative humidity and temperature. *PLOS Pathog.* **3**, 1470–1476 (2007). [doi:10.1371/journal.ppat.0030151](https://doi.org/10.1371/journal.ppat.0030151) [Medline](#)

12. J. Shaman, V. E. Pitzer, C. Viboud, B. T. Grenfell, M. Lipsitch, Absolute humidity and the seasonal onset of influenza in the continental United States. *PLOS Biol.* **8**, e1000316 (2010). [doi:10.1371/journal.pbio.1000316](https://doi.org/10.1371/journal.pbio.1000316) Medline
13. R. E. Baker, A. S. Mahmud, C. E. Wagner, W. Yang, V. E. Pitzer, C. Viboud, G. A. Vecchi, C. J. E. Metcalf, B. T. Grenfell, Epidemic dynamics of respiratory syncytial virus in current and future climates. *Nat. Commun.* **10**, 5512 (2019). [doi:10.1038/s41467-019-13562-y](https://doi.org/10.1038/s41467-019-13562-y) Medline
14. V. E. Pitzer, C. Viboud, W. J. Alonso, T. Wilcox, C. J. Metcalf, C. A. Steiner, A. K. Haynes, B. T. Grenfell, Environmental drivers of the spatiotemporal dynamics of respiratory syncytial virus in the United States. *PLOS Pathog.* **11**, e1004591 (2015). [doi:10.1371/journal.ppat.1004591](https://doi.org/10.1371/journal.ppat.1004591) Medline
15. M. E. Martinez, The calendar of epidemics: Seasonal cycles of infectious diseases. *PLOS Pathog.* **14**, e1007327 (2018). [doi:10.1371/journal.ppat.1007327](https://doi.org/10.1371/journal.ppat.1007327) Medline
16. S. Takahashi, Q. Liao, T. P. Van Boeckel, W. Xing, J. Sun, V. Y. Hsiao, C. J. E. Metcalf, Z. Chang, F. Liu, J. Zhang, J. T. Wu, B. J. Cowling, G. M. Leung, J. J. Farrar, H. R. van Doorn, B. T. Grenfell, Hand, foot, and mouth disease in China: Modeling epidemic dynamics of enterovirus serotypes and implications for vaccination. *PLOS Med.* **13**, e1001958 (2016). [doi:10.1371/journal.pmed.1001958](https://doi.org/10.1371/journal.pmed.1001958) Medline
17. J. R. Gog, S. Ballesteros, C. Viboud, L. Simonsen, O. N. Bjornstad, J. Shaman, D. L. Chao, F. Khan, B. T. Grenfell, Spatial transmission of 2009 pandemic influenza in the US. *PLOS Comput. Biol.* **10**, e1003635 (2014). [doi:10.1371/journal.pcbi.1003635](https://doi.org/10.1371/journal.pcbi.1003635) Medline
18. S. M. Kissler, C. Tedijanto, E. Goldstein, Y. H. Grad, M. Lipsitch, Projecting the transmission dynamics of SARS-CoV-2 through the postpandemic period. *Science* eabb5793 (2020). [doi:10.1126/science.abb5793](https://doi.org/10.1126/science.abb5793) Medline
19. Centers for Disease Control and Prevention, Surveillance for common human coronaviruses (2020); www.cdc.gov/surveillance/nrevss/coronavirus/index.html.
20. L. Hoffmann, G. Günther, D. Li, O. Stein, X. Wu, S. Griessbach, Y. Heng, P. Konopka, R. Müller, B. Vogel, J. S. Wright, From ERA-Interim to ERA5: The considerable impact of ECMWF's next-generation reanalysis on Lagrangian transport simulations. *Atmos. Chem. Phys.* **19**, 3097–3124 (2019). [doi:10.5194/acp-19-3097-2019](https://doi.org/10.5194/acp-19-3097-2019)
21. NASA Socioeconomic Data and Applications Center (SEDAC), Gridded Population of the World, Version 4 (GPWv4): Population Density, Revision 11. Palisades, NY; <https://sedac.ciesin.columbia.edu/data/set/gpw-v4-population-density-rev11> [accessed March 2020].
22. S. W. Park, B. M. Bolker, D. Champredon, D. J. D. Earn, M. Li, J. S. Weitz, B. T. Grenfell, J. Dushoff, Reconciling early-outbreak estimates of the basic reproductive number and its uncertainty: framework and applications to the novel coronavirus (SARS-CoV-2) outbreak. medRxiv 2020.01.30.20019877 [Preprint]. 28 February 2020; <https://doi.org/10.1101/2020.01.30.20019877>.
23. M. Kamo, A. Sasaki, The effect of cross-immunity and seasonal forcing in a multi-strain epidemic model. *Physica D* **165**, 228–241 (2002). [doi:10.1016/S0167-2789\(02\)00389-5](https://doi.org/10.1016/S0167-2789(02)00389-5)

24. J. D. Tamerius, J. Shaman, W. J. Alonso, K. Bloom-Feshbach, C. K. Uejio, A. Comrie, C. Viboud, Environmental predictors of seasonal influenza epidemics across temperate and tropical climates. *PLOS Pathog.* **9**, e1003194 (2013). [doi:10.1371/journal.ppat.1003194](https://doi.org/10.1371/journal.ppat.1003194) [Medline](#)
25. R. E. Baker, rebaker64/climate-cov: R1. Zenodo (2020); [doi:10.5281/zenodo.3787766](https://doi.org/10.5281/zenodo.3787766).
26. M. E. Killerby, H. M. Biggs, A. Haynes, R. M. Dahl, D. Mustaquim, S. I. Gerber, J. T. Watson, Human coronavirus circulation in the United States 2014–2017. *J. Clin. Virol.* **101**, 52–56 (2018). [doi:10.1016/j.jcv.2018.01.019](https://doi.org/10.1016/j.jcv.2018.01.019) [Medline](#)
27. R. Gelaro, W. McCarty, M. J. Suárez, R. Todling, A. Molod, L. Takacs, C. Randles, A. Darmenov, M. G. Bosilovich, R. Reichle, K. Wargan, L. Coy, R. Cullather, C. Draper, S. Akella, V. Buchard, A. Conaty, A. da Silva, W. Gu, G.-K. Kim, R. Koster, R. Lucchesi, D. Merkova, J. E. Nielsen, G. Partyka, S. Pawson, W. Putman, M. Rienerer, S. D. Schubert, M. Sienkiewicz, B. Zhao, The Modern-Era Retrospective Analysis for Research and Applications, Version 2 (MERRA-2). *J. Clim.* **30**, 5419–5454 (2017). [doi:10.1175/JCLI-D-16-0758.1](https://doi.org/10.1175/JCLI-D-16-0758.1) [Medline](#)
28. L. Bao, W. Deng, H. Gao, C. Xiao, J. Liu, J. Xue, Lv. Qi, J. Liu, P. Yu, Y. Xu, F. Qi, Y. Qu, F. Li, Z. Xiang, H. Yu, S. Gong, M. Liu, G. Wang, S. Wang, Z. Song, Y. Liu, W. Zhao, Y. Han, L. Zhao, X. Liu, Q. Wei, C. Qin, Lack of reinfection in rhesus macaques infected with SARS-CoV-2. bioRxiv 2020.03.13.990226 [Preprint]. 1 May 2020; <https://doi.org/10.1101/2020.03.13.990226>.
29. K. A. Callow, H. F. Parry, M. Sergeant, D. A. Tyrrell, The time course of the immune response to experimental coronavirus infection of man. *Epidemiol. Infect.* **105**, 435–446 (1990). [doi:10.1017/S0950268800048019](https://doi.org/10.1017/S0950268800048019) [Medline](#)